Transport and Dispersion of Nanoparticles in Periodic Nanopost Arrays

Kai He,[†] Scott T. Retterer,[‡] Bernadeta R. Srijanto,[§,∥] Jacinta C. Conrad,[†,*] and Ramanan Krishnamoorti[†,*]

[†]Department of Chemical and Biomolecular Engineering, University of Houston, Houston, Texas 77204-4004, United States, [‡]Center for Nanophase Materials Sciences and BioSciences Divisions and [§]Center for Nanophase Materials Sciences, Oak Ridge National Laboratory, Oak Ridge, Tennessee 37934, United States, and [∥]Department of Materials Science & Engineering, University of Tennessee, Knoxville, Tennessee 37996, United States

ABSTRACT Nanoparticles transported through highly confined porous media exhibit faster breakthrough than small molecule tracers. Despite important technological applications in advanced materials, human health, energy, and environment, the microscale mechanisms leading to early breakthrough have not been identified. Here, we measure dispersion of nanoparticles at the single-particle scale in regular arrays of nanoposts and show that for highly confined flows of dilute suspensions of nanoparticles the longitudinal and transverse velocities exhibit distinct scaling behaviors. The distributions of transverse particle velocities become narrower and more non-Gaussian when the particles are strongly confined. As a result, the transverse dispersion of highly confined nanoparticles at low Péclet numbers is significantly less important than longitudinal dispersion, leading to early breakthrough. This finding suggests a fundamental mechanism by which to control dispersion and thereby improve efficacy of nanoparticles applied for advanced polymer nanocomposites, drug delivery, hydrocarbon production, and environmental remediation.

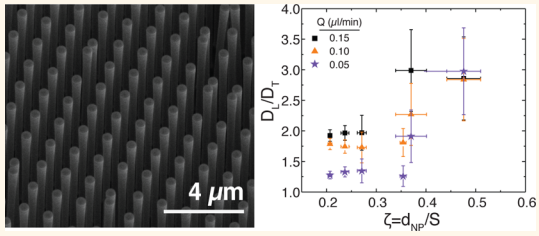

KEYWORDS: nanoparticles · transport · dispersion · structured media

Dispersion affects applications, including nanocomposite processing, drug delivery, natural resource extraction, environmental remediation, and water treatment, that require nanometer-sized particles to be transported through complex and often confining media. In polymer nanocomposite processing, nanoparticles suspended in polymer resins must be efficiently dispersed to obtain optimal mechanical and physical properties and eliminate stress concentrators.[1,2] In cancer therapeutics, nanoparticles must be efficiently transported through the vascular and lymphatic systems and the extracellular matrix to reach targeted tumors in the body.[3−8] Similarly, for enhanced oil recovery nanomaterials used to increase the viscosity of sweep fluids[9] must be transported to regions of low permeability in natural porous media.[10] Dispersion reduces the efficacy of these strategies, as spreading nanoparticles[11] fail to reach targeted sites. Conversely, nanoparticles transport contaminants in saturated soils[12] and thereby exacerbate environmental damage, and biological nanoparticles such as bacteriophage or other viruses contaminate drinking-water aquifers.[13] These scenarios share a common feature: the characteristic pore size in the media is comparable to the size of the nanoparticles, so that the nanoparticles are highly confined. Controlling the spread of nanoparticles in complex and confined geometries thus requires understanding the mechanisms of nanoparticle dispersion in this limit.

The transport of small solutes in porous media is typically described by the convective-diffusion equation, $D_L(\partial^2C/\partial z^2) + (1/r)(\partial/\partial r)(D_T r(\partial C/\partial r)) = u(\partial C/\partial z) + (\partial C/\partial t)$, where C is the average concentration of solute, u is the mean velocity of the fluid, and D_L and D_T are the diffusion coefficients in the streamwise (longitudinal) and cross-stream (transverse) directions. The ratio of D_L or D_T to the molecular diffusion coefficient D_m characterizing the extent of solute dispersion depends upon the molecular Péclet number $Pe_m = ud/D_m$, where d is a typical length scale, such as the particle diameter or the spacing between voids.

* Address correspondence to jcconrad@uh.edu, ramanan@uh.edu.

Received for review August 28, 2013 and accepted April 16, 2014.

Published online April 16, 2014
10.1021/nn404497z

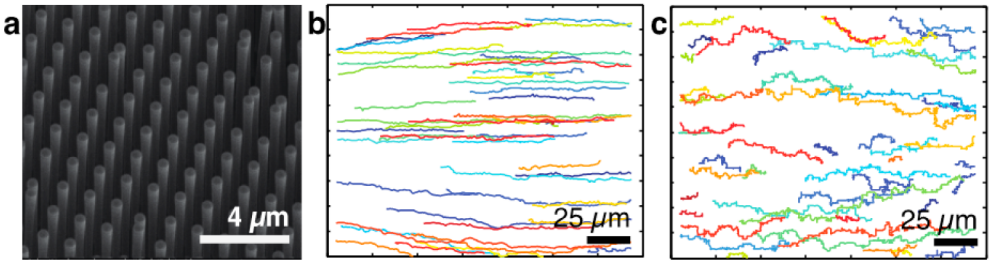

Figure 1. (a) Electron micrograph of posts of diameter d_p = 500 nm and spacing S = 0.8 μm. For the series of post arrays described here d_p is constant and S varies from 0.8 to 2.0 μm. (b) and (c): Representative trajectories of 400 nm particles transported through post arrays with $\zeta = d_{NP}/S$ = 0.25 at a bulk flow rate Q = 0.15 μL/min, corresponding to Péclet number Pe_x = 58.9, and ζ = 0.48 at Q = 0.05 μL/min, corresponding to Pe_x = 2.2.

In macroscopic experiments, which typically measure bulk quantities such as concentration profiles,[14] the ratios D_L/D_m and D_T/D_m are nearly constant and approximately equal at small values of Pe_m, suggesting that diffusion dominates in this limit. Models of solute dispersion developed for different pore geometries, including both ordered[15] and disordered media,[16,17] have focused on the scaling behavior of macroscale dispersion at large values of Pe_m, where both D_L/D_m and D_T/D_m increase for $Pe_m > 1$ and mechanical dispersion dominates.

Models developed for small solutes, however, may not adequately describe the transport properties of nanoparticles. As one example, noninteracting nanoparticles are excluded by their finite size from the immediate vicinity of pore surfaces[18] and therefore cannot access the slow streamlines near surfaces required by no-slip boundary conditions.[19] As a result, particles are restricted to fast streamlines and can exhibit higher velocities than that of the solvent, which manifests on the macroscale as early breakthrough.[20] This principle underlies applications in separations, including hydrodynamic chromatography[21] and deterministic lateral transport.[22,23] These and similar results confirm that microscale mechanisms of transport for nanoparticles differ from those of solutes. Despite the ubiquity of nanoparticle transport in practical applications, however, the connection between microscale and bulk transport properties of nanoparticles in confined porous media remains elusive.

In this paper, we show that confinement modifies the microscale transport properties of nanoparticles in an ordered array of nanoposts that act to confine the nanoparticles. We used fluorescence microscopy and particle tracking algorithms to obtain trajectories of nanoparticles of diameter 400 nm as they were transported through square arrays of nanoposts in which the edge-to-edge spacing of posts was 0.8–2 μm. As the particles are increasingly confined by the posts, the characteristic velocities for dispersion parallel to and perpendicular to the direction of flow become slower and become increasingly different from each other. The longitudinal dispersion velocities are nearly Gaussian-distributed, and the mean longitudinal dispersion velocity is consistent with a constant pressure drop across each array of nanoposts. The transverse velocity distributions, however, become increasingly stretched and exponential as confinement is increased. Stretched distributions appear only when the nanoparticles are strongly confined, and nanoparticles trapped inside pores preferentially travel along the fast streamlines running through the pore centers. Confinement thus enhances the spread of noninteracting nanoparticles along the direction of flow and suppresses their dispersion normal to flow. Because nanoparticles become slower as confinement is increased, the strongly confined limit corresponds to the limit of low Péclet number Pe. Our results are thus in sharp contrast to those seen for small molecule solutes, in which longitudinal and transverse dispersion are approximately equal at low Pe.

RESULTS AND DISCUSSION

To study nanoparticle dispersion in controlled models of porous media, we created square arrays of silicon nanoposts in microfluidic chips (Figure 1a) and applied a pressure gradient along one axis of the square array (set by the fabrication process and verified by SEM) to drive the flow of nanoparticle suspensions through the post arrays. The shape of the trajectories of nanoparticles transported through these nanopost arrays becomes increasingly tortuous as Pe_x is decreased, as shown for two extreme cases in Figure 1a, b. The change in trajectory shape reflects the increasing importance of diffusion: convection dominates at large Pe_x, leading to straight trajectories, whereas at small Pe_x diffusion becomes increasingly important, leading to tortuous trajectories. We note that even at small Pe_x fewer than 2% of all particles in the focal volume enter or leave the focal volume from outside the plane of focus (that is, vertically) during the entire time over which the particles are tracked. To capture this transition, we examine two metrics that describe the loss of directional persistence of the particles: the average tortuosity $\langle T \rangle$ and the average of the cosine of the angle between velocity vectors $\langle \cos \chi \rangle$ (Figure 2a, b). As Pe_x is decreased, the tortuosity of the trajectories increases and the velocity

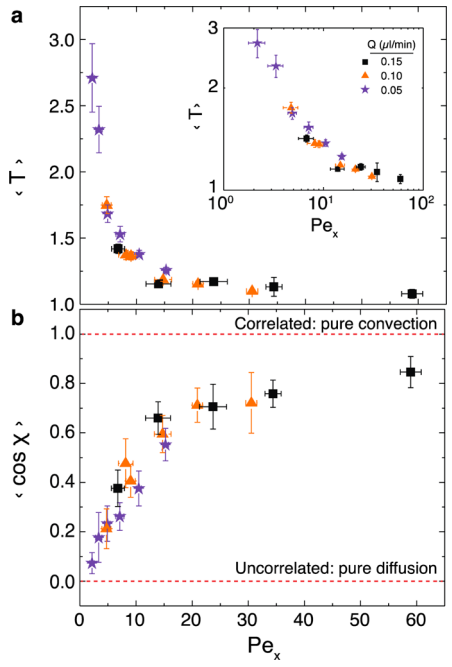

Figure 2. (a) Average tortuosity $\langle T \rangle$ and (b) average angle between velocity vectors $\langle \cos \chi \rangle$ as a function of Péclet number Pe_x for 400 nm particles transported through post arrays. The inset to (a) shows $\langle T \rangle$ as a function of Pe_x on logarithmic axes. In (b) the dashed lines indicate the limits expected for pure convection ($\langle \cos \chi \rangle = 1$) and for pure diffusion ($\langle \cos \chi \rangle = 0$), respectively. Horizontal error bars indicate uncertainty in the measured post spacing; vertical error bars indicate uncertainty associated with the fitting of the velocity distributions.

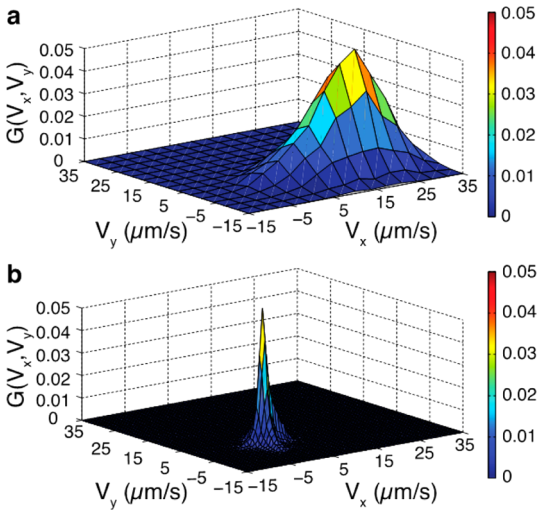

Figure 3. 2-D probability distributions of velocity $G(V_x, V_y)$ for 400 nm particles transported through post arrays for (a) confinement parameter $\zeta = 0.21$ at a bulk flow rate $Q = 0.15$ μL/min ($Pe_x = 58.9$) and (b) $\zeta = 0.48$ at $Q = 0.05$ μL/min ($Pe_x = 2.1$).

vectors become increasingly uncorrelated, consistent with the increased importance of diffusion.

To obtain insight into the microscale mechanisms underlying this transition, we first examine the two-dimensional probability distribution $G(V_x,V_y)$ of velocities along (V_x) and normal to (V_y) the direction of flow (Figure 3a, b). At low Pe_x, $G(V_x,V_y)$ is roughly symmetric in both directions, indicating that diffusive transport dominates on the microscale. As Pe_x is increased, this symmetry is broken along the direction of flow (V_x), reflecting the increased contribution from convective transport.

We assess the effects of confinement on microscale transport processes in the longitudinal and transverse directions by separating the two-dimensional probability distribution function into the one-dimensional velocity distributions $G(V_x)$ and $G(V_y)$. When the posts are widely spaced, $G(V_x)$ is approximately Gaussian and the location of the maximum corresponds to the average convective velocity of the particles (Figure 4a). As the spacing between the posts is decreased, the maximum in $G(V_x)$ shifts to smaller values of V_x, consistent with slowing of transport along the direction of flow induced by the posts. In addition, a second local maximum in $G(V_x)$ centered approximately at zero emerges in highly confined geometries, corresponding to particles that are trapped within the interstitial space between the posts. To quantify these observations, we fit $G(V_x)$ with the sum of two Gaussian functions

$$G(V_x) = C_1 \exp\left[-\left(\frac{|V_x|}{v}\right)^2\right] + C_2 \exp\left[-\left(\frac{V_x - \langle V_x \rangle}{\delta}\right)^2\right] \quad (1)$$

where C_1 and C_2 are prefactors and v and δ are characteristic velocities for each process (Supporting Information). The first term of eq 1 captures the population of particles that are caged by the pores,[24] and the second term captures those particles transported through the post array. This analysis allows us to systematically obtain the characteristic width of the velocity distribution δ of the particles that are transported along the direction of flow, which is related to longitudinal dispersion. An alternate analysis of the data using a traditional convection–diffusion model,[25] which neglects adsorption, cannot account for heterogeneous (i.e., bimodal) distribution of particle mobility. Moreover, in the highly confined systems studied here the diffusive dynamics of the particles become increasingly non-Gaussian and the traditional convection–diffusion analysis neglects that factor.

Across a range of confinements and bulk flow rates, we find that the average velocity $\langle V_x \rangle$ scales with the confinement parameter as $\langle V_x \rangle \sim \zeta^{-2}$ (Figure 4b) and increases approximately linearly with Q (Figure 4c). Equality of pressure drop across each of the arrays (Supporting Information) requires the velocity of the *fluid* within each array to scale inversely with the area occupied by the posts and $\langle V_x \rangle \sim S^2 \sim \zeta^{-2}$, in accord with our observations. The characteristic longitudinal velocity δ scales with confinement parameter as $\delta \sim \zeta^{-1}$ and again decreases approximately linearly with the flow rate, indicating that along the flow

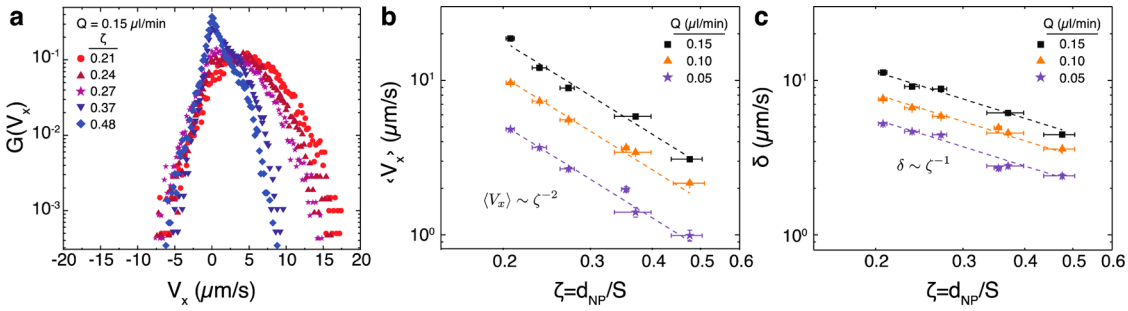

Figure 4. (a) 1-D probability distributions of velocities $G(V_x)$ for nanoparticles transported through post arrays with $\zeta = 0.21$ (red circles), 0.24 (maroon upright triangles), 0.27 (purple stars), 0.37 (royal blue downward triangles), and 0.48 (blue diamonds) at bulk flow rate $Q = 0.15$ μL/min. As the spacing between the posts is decreased, the velocities along the flow become slower and the distributions shift to the left. (b) Average velocity $\langle V_x \rangle$ and (c) characteristic velocity δ obtained from fits of $G(V_x)$ to eq 1 as a function of ζ for nanoparticles transported through post arrays at $Q = 0.05$ (purple stars), 0.10 (orange triangles), and 0.15 (black squares) μL/min. Dashed lines in (b) and (c) indicate fits to power-law models as indicated in the panels, and best fits suggest that $\langle V_x \rangle \sim \zeta^{-(2\pm0.2)}$ and $\delta \sim \zeta^{-(1\pm0.2)}$. Horizontal error bars in (b) and (c) indicate uncertainty in the measured post spacing; vertical error bars indicate uncertainty associated with the fitting of the velocity distributions (for flow).

direction the dominant process for dispersion is Fickian diffusion of nanoparticles.

The distribution of velocities in the transverse direction ($G(V_y)$) is symmetric and centered at zero for all S and Q (Figure 5a), showing that particles exhibit no preferred direction normal to the flow. We separately note that, even at the slowest flow rates studied and over the entire duration of the experiments, only a few particles enter or exit the focal volume by moving vertically. The shape of this distribution, however, becomes increasingly non-Gaussian as the confinement is increased. We note that similar non-Gaussian behavior has also been observed for micrometer sized particles flowing in three-dimensional random porous media.[26,27] Here, the distributions of velocity are best fit by a stretched Gaussian model[28]

$$G(V_y) = C_3 \exp\left[-\left(\frac{|V_y|}{\gamma}\right)^{\beta}\right] \qquad (2)$$

where C_3 is a prefactor and γ is a characteristic velocity (Supporting Information). Both the characteristic velocity γ (Figure 5b) and the stretching exponent β (Figure 5c) decrease as the particles are increasingly confined, consistent with dynamics that are increasingly slow and heterogeneous. The stretching exponents are smaller than those measured for quiescent diffusion of the nanoparticles in these confined media, however, indicating that confinement alone cannot be responsible for these dynamics.

The longitudinal (δ) and transverse (γ) velocities characterize the widths of the velocity distributions in these directions. To relate these microscopic characteristic velocities to dispersion, we estimate longitudinal and transverse dispersion coefficients as $D_L = \delta S$ and $D_T = \gamma S$, respectively. These measures of the dispersion coefficients suggest that the squared fluctuations in the position of the particles grow linearly with the velocity,[29] and we choose the post spacing as a characteristic geometric length scale. We observe that D_L (normalized by the quiescent diffusivity D_q) scales across the range of accessible Pe_x as a power law (Figure 6a) and is independent of flow rate. The collapse of the data onto a master curve supports the microscopic definitions of D_L and Pe_x employed here. The observed power law dependence is consistent with that observed for bulk dispersion in periodic two-dimensional porous media over similar ranges of Peclet numbers.[30]

The normalized transverse dispersion coefficient (D_T/D_q) also scales as a power law ($\sim Pe_x^{0.5}$) at large values of Pe_x. At modest values of Pe_x, however, D_T/D_q *does not* collapse on to a master curve (Figure 6b). This result *sharply contrasts* with transverse dispersion for small solutes,[31] in which a dominant diffusively coupled process allows the transverse dispersion coefficients to be scaled onto a master curve. We thus hypothesize that confinement underpins the deviations from scaling collapse. To explore the role of confinement on transverse dispersion, we examine the ratio of dispersion coefficients D_L/D_T as a function of ζ in Figure 7a. At small values of ζ, the ratio of longitudinal to transverse dispersivities is independent of ζ and scales with flow rate, indicating that similar mechanisms that also scale with flow rate dominate both dispersion processes. At large ζ and extreme confinement, which in our experiments corresponds to low Pe_x (Figure 7b), at most one nanoparticle can reside in the interstitial pore defined by a square of four nanoposts and the ratio of D_L/D_T increases significantly. By contrast, previous studies of small molecule tracers in simple fluids showed that at small Pe_x the ratio of D_L/D_T should approach unity.[32−35] The divergence of the ratio of D_L/D_T for strongly confined flows of nanoparticles corresponding to low Peclet number shown in Figure 7b and the previously observed master curve for the longitudinal dispersion together suggest that the deviation of the transverse dispersion from the expected scaling arises from the interplay of flow and confinement.

The strikingly non-Gaussian and stretched distributions of velocity in the transverse direction to flow that

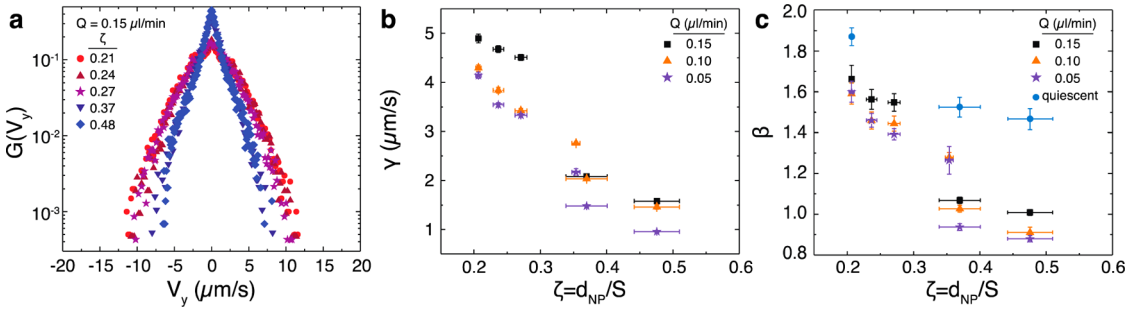

Figure 5. (a) 1-D probability distributions of velocities $G(V_y)$ for 400 nm nanoparticles transported through post arrays with confinement parameter ζ = 0.21 (red circles), 0.24 (maroon upright triangles), 0.27 (purple stars), 0.37 (royal downward triangles), and 0.48 (blue diamonds) at Q = 0.15 μL/min. Velocities normal to the flow direction become more narrowly distributed and non-Gaussian as the confinement is increased. (b) Characteristic velocity γ and (c) stretching exponent β, obtained from fits of $G(V_y)$ to eq 2, as a function of ζ for nanoparticles transported through post arrays at Q = 0.05 (purple stars), 0.10 (orange triangles), and 0.15 (black squares) μL/min and in quiescent state (blue circles). Horizontal error bars in (b) and (c) indicate uncertainty in the measured post spacing; vertical error bars indicate uncertainty associated with the fitting of the velocity distributions (for flow) or displacement distributions (for quiescent state).

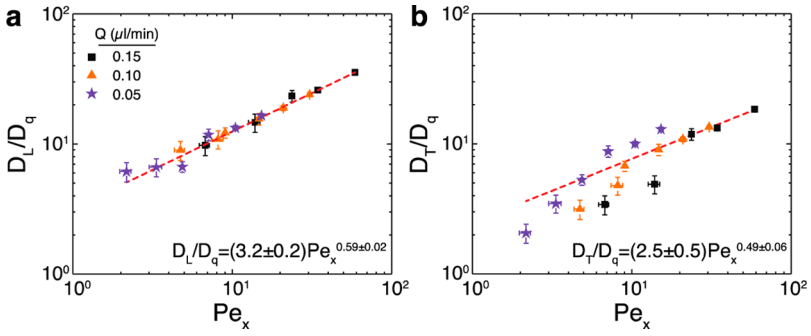

Figure 6. (a) Ratio of longitudinal diffusivity to quiescent diffusivity D_L/D_q as a function of Péclet number Pe_x for 400 nm particles transported through post arrays. Red line indicates fit to a power-law model. (b) Ratio of transverse diffusivity to quiescent diffusivity D_T/D_q as a function of Pe_x for 400 nm particles transported through post arrays. Red line indicates fit to a power-law model. Horizontal error bars indicate uncertainty in the measured post spacing; vertical error bars indicate uncertainty associated with the fitting of the velocity distributions.

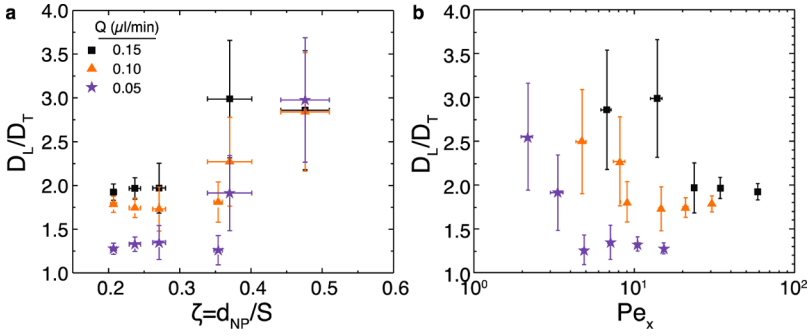

Figure 7. (a) Ratio of longitudinal and transverse diffusivities D_L/D_T as a function of confinement parameter ζ for 400 nm particles transported through post arrays. (b) Ratio of longitudinal and transverse diffusivities D_L/D_T as a function of Péclet number Pe_x for 400 nm particles transported through post arrays. Symbols indicate bulk flow rates of Q = 0.05 (purple stars), 0.10 (orange triangles), and 0.15 (black squares) μL/min. D_L/D_T is nearly constant at small ζ (large Pe_x) and increases significantly at higher values of ζ (small Pe_x).

appear when particles are strongly confined.[36−38] We suggest a simple physical picture for the origins of these distributions. When the particle diameter is comparable to typical pore and throat sizes, only one particle can instantaneously occupy a pore. The transport of particles between pores must therefore be sequential: a particle entering an occupied pore must wait for the previous occupant to exit. Longitudinal dispersion is largely unaffected as the nanoparticles preferentially occupy the faster streamlines and the imposed flow dominates over diffusive dynamics for all conditions studied. Transverse dispersion, however, is significantly impacted by the confinement induced by the posts. This deviation is most pronounced when diffusive transport is dominant, i.e., at small Pe_x as shown in Figure 7b, as also suggested by the decrease in stretching exponent compared to

that expected for quiescent nanoparticles in nanopost arrays (Figure 5c). We anticipate that these effects would be significantly magnified at higher concentrations of nanoparticles than those used in the current study.

CONCLUSIONS

Our results suggest new features of microscale dispersion of nanoparticles in porous media where the confinement imposed by the medium is strongly coupled to the externally imposed flow. The characteristic longitudinal and transverse velocities for dispersion exhibit distinct scaling behaviors as the particles are increasingly confined, with the transverse velocity distributions becoming increasingly stretched and exponential. These features appear only in highly confined media, in which a single particle trapped inside a pore prefers to ride along the fast streamlines, and results in longitudinal dispersion dominating over transverse dispersion. Confinement thus enhances dispersion of noninteracting nanoparticles in the direction of flow and suppresses transverse dispersion through nanoporous media. This effect, along with other well-studied phenomena such as the size exclusion of larger particles from small pores, leads to early breakthrough of nanoparticles compared to tracers in realistic porous media in which the pore or pore-throat sizes are comparable to the size of the nanoparticles. Selecting particles to obtain enhanced longitudinal dispersion could lead to improved efficacy of nanoparticles as applied for development of advanced composite materials that effectively eliminate stress concentrators,[1,2] for drug delivery to the deep lung,[4] mucus environments[6] and the brain,[7] for *in situ* catalysis[39] in environmental remediation applications,[12] and for controlled rheological fluids for improved exploration and production of hydrocarbons.[9]

METHODS

Nanoparticle Disperions. Fluo-max dyed red aqueous fluorescent polystyrene particles with diameter (d_{NP}) of 400 nm, purchased from Thermo Fisher, were diluted with deuterium oxide (Sigma-Aldrich) to a volume fraction of $\varphi = 1 \times 10^{-4}$, corresponding to a number density of 2.8×10^9 mL^{-1}. Because of the geometry of the system, a significantly lower particle concentration is observed in the post arrays. At these concentrations we expect that hydrodynamic interactions between particles to be minimal. A detailed description of these materials and the protocol for sample preparation can be found in ref 40.

Fabrication and Characterization of Cylindrical Nanopost Arrays. We fabricated individual arrays of cylindrical nanoposts,[41] of area of 250 μm $\times$ 250 μm and uniformly arranged along a silicon microchannel of length 2 mm and width 800 μm, in which the posts (diameter 500 nm and height 10 μm) were separated by constant spacing (S) ranging from 0.8 to 2 μm. A detailed description of the fabrication protocol for these arrays is given in ref 28.

Imaging of Dispersions in Nanopost Arrays. We imaged the nanoparticles in these model media, in which the dimensionless confinement parameter $\zeta = d_{NP}/S$ ranged from 0.2 to 0.48, both in quiescent conditions and in flow. For both quiescent (diffusion) and flow (dispersion) experiments, microchannels were incorporated into PDMS-based microfluidic devices. The height of the channels was 10 μm, and because of the adhesion between the PDMS device and the silicon based posts the particles in the nanopost array could not escape vertically out of the cylindrical post array. The focal plane for the imaging was set at approximately the midpoint of the post height (i.e., at a height of $\sim$5 μm above the bottom surface of the microchannel) to minimize any surface induced phenomena. Flow was driven in dispersion experiments by a syringe pump (Harvard Apparatus, Pump 11 Pico Plus Elite) at three different bulk flow rates (Q). The flow was driven along one of the principle axes of the square arrays. We note that few particles enter or leave the focal volume in the vertical direction, even at the lowest flow rates measured. Nanoparticles were imaged on an Olympus BX51 upright microscope equipped with a 50$\times$ objective (Olympus LMPlanFl N, numerical aperture of 0.5) using a Qiclick digital CCD camera (QIClick-F-M-12, Canada) controlled by StreamPix 5 software (Norpix, Canada), which yielded a pixel size of 0.258 $\pm$ 0.002 μm/pixel. For each diffusion experiment, we collected 1000 images of area 179.6 μm $\times$ 134.2 μm (corresponding to 696 pixels $\times$520 pixels) at a frame rate of 10 frames per second (fps).

Particle Tracking and Trajectory Shape Metrics. We used a single particle-tracking (SPT) algorithm to track the nanoparticles over time.[42] From the trajectories of individual nanoparticles, we calculated the distribution of velocities $G(V_x,V_y)$ and thereby extracted the average velocity along the direction of flow $\langle V_x \rangle$. Velocity distributions were calculated using time steps of 0.1, 0.2, 0.3, and 0.4 s and shown to be independent of time step for short time steps (Supporting Information, Figure S1). We therefore used $\Delta t = 0.1$ s as the time step over which to calculate velocities. We also measured the quiescent state diffusivity D_q of nanoparticles in the post arrays as a function of post spacing (Supporting Information) and therefore obtained a Péclet number $Pe_x = \langle V_x \rangle S/D_q$. We characterized the shape of the trajectories *via* the long-time limits of the correlation angle $\cos \chi = (V_i \cdot V_j)/|V_i||V_j|$ and the tortuosity $T(n\delta t) = \sum_{i=1}^{n} L_i/\Delta L_n$. Here, V_i and V_j are the velocities at two widely spaced points (x_i,y_i) and (x_j,y_j) in a single trajectory, L_i is the distance between two points on a trajectory separated by a single time step δt, and ΔL_n is the end-to-end distance between two points separated by n timesteps.

Conflict of Interest: The authors declare no competing financial interest.

Acknowledgment. This publication is based on work supported in part by Award No. KUS-C1-018-02, made by King Abdullah University of Science and Technology (KAUST). R.K. and K.H. acknowledge the partial support of the Gulf of Mexico Research Initiative (Consortium for Ocean Leadership Grant SA 12-05/GoMRI-002). J.C.C. is supported by the American Chemical Society Petroleum Research Fund (52537-DNI7) and the National Science Foundation (DMR-1151133). A portion of this research was conducted at the Center for Nanophase Materials Sciences, which is sponsored at Oak Ridge National Laboratory by the Scientific User Facilities Division, Office of Basic Energy Sciences, U.S. Department of Energy.

Supporting Information Available: Extended materials and methods, characterization of the nanopost arrays, and additional discussion. This material is available free of charge *via* the Internet at http://pubs.acs.org.

REFERENCES AND NOTES

1. Kumar, S. K.; Krishnamoorti, R. Nanocomposites: Structure, Phase Behavior, and Properties. *Annu. Rev. Chem. Biomol. Eng.* **2010**, *1*, 37–58.
2. Njuguna, J.; Pielichowski, K.; Alcock, J. R. Epoxy-Based Fibre Reinforced Nanocomposites. *Adv. Eng. Mater.* **2007**, *9*, 835–847.
3. Gulyaev, A. E.; Gelperina, S. E.; Skidan, I. N.; Antropov, A. S.; Kivman, G. Y.; Kreuter, J. Significant Transport of Doxorubicin

into the Brain with Polysorbate 80-Coated Nanoparticles. *Pharm. Res.* **1999**, *16*, 1564–1569.
4. Singh, R.; Lillard, J. W., Jr. Nanoparticle-Based Targeted Drug Delivery. *Exp. Mol. Pathol.* **2009**, *86*, 215–223.
5. Chan, J. M.; Zhang, L. F.; Tong, R.; Ghosh, D.; Gao, W. W.; Liao, G.; Yuet, K. P.; Gray, D.; Rhee, J. W.; Cheng, J. J.; et al. Spatiotemporal Controlled Delivery of Nanoparticles to Injured Vasculature. *Proc. Natl. Acad. Sci. U.S.A.* **2010**, *107*, 2213–2218.
6. Lai, S. K.; Wang, Y. Y.; Hida, K.; Cone, R.; Hanes, J. Nanoparticles Reveal that Human Cervicovaginal Mucus is Riddled with Pores Larger than Viruses. *Proc. Natl. Acad. Sci. U.S.A.* **2010**, *107*, 598–603.
7. Liu, H. L.; Hua, M. Y.; Yang, H. W.; Huang, C. Y.; Chu, P. C.; Wu, J. S.; Tseng, I. C.; Wang, J. J.; Yen, T. C.; Chen, P. Y.; et al. Magnetic Resonance Monitoring of Focused Ultrasound/Magnetic Nanoparticle Targeting Delivery of Therapeutic Agents to the Brain. *Proc. Natl. Acad. Sci. U.S.A.* **2010**, *107*, 15205–15210.
8. Wong, C.; Stylianopoulos, T.; Cui, J. A.; Martin, J.; Chauhan, V. P.; Jiang, W.; Popovic, Z.; Jain, R. K.; Bawendi, M. G.; Fukumura, D. Multistage Nanoparticle Delivery System for Deep Penetration into Tumor Tissue. *Proc. Natl. Acad. Sci. U.S.A.* **2011**, *108*, 2426–2431.
9. Metin, C.; Bonnecaze, R.; Nguyen, Q. The Viscosity of Silica Nanoparticle Dispersions in Permeable Media. *SPE Reservoir Eval. Eng.* **2013**, *16*, 327–332.
10. Sahimi, M. Flow Phenomena in Rocks: From Continuum Models to Fractals, Percolation, Cellular Automata, and Simulated Annealing. *Rev. Mod. Phys.* **1993**, *65*, 1393–1534.
11. Wasan, D. T.; Nikolov, A. D. Spreading of Nanofluids on Solids. *Nature* **2003**, *423*, 156–159.
12. Fang, J.; Shan, X.-q.; Wen, B.; Lin, J.-M.; Owens, G. Stability of Titania Nanoparticles in Soil Suspensions and Transport in Saturated Homogeneous Soil Columns. *Environ. Pollut.* **2009**, *157*, 1101–1109.
13. Zhang, W. X. Nanoscale Iron Particles for Environmental Remediation: An Overview. *J. Nanopart. Res.* **2003**, *5*, 323–332.
14. Eidsath, A.; Carbonell, R.; Whitaker, S.; Herrmann, L. Dispersion in Pulsed Systems—III: Comparison Between Theory and Experiments for Packed Beds. *Chem. Eng. Sci.* **1983**, *38*, 1803–1816.
15. Brenner, H. Dispersion Resulting from Flow through Spatially Periodic Porous Media. *Philos. Trans. R. Soc. A* **1980**, *297*, 81–133.
16. Koch, D.; Brady, J. Dispersion in Fixed Beds. *J. Fluid. Mech.* **1985**, *154*, 399–427.
17. Saffman, P. A Theory of Dispersion in a Porous Medium. *J. Fluid. Mech.* **1959**, *6*, 321–349.
18. DiMarzio, E.; Guttman, C. Separation by Flow. *Macromolecules* **1970**, *3*, 131–146.
19. Auset, M.; Keller, A. A. Pore-Scale Processes that Control Dispersion of Colloids in Saturated Porous Media. *Water Resour. Res.* **2004**, *40*, W03503.
20. Bales, R.; Gerba, C.; Grondin, G.; Jensen, S. Bacteriophage Transport in Sandy Soil and Fractured Tuff. *Appl. Environ. Microb.* **1989**, *55*, 2061–2067.
21. Blom, M.; Chmela, E.; Oosterbroek, R.; Tijssen, R.; van den Berg, A. On-Chip Hydrodynamic Chromatography Separation and Detection of Nanoparticles and Biomolecules. *Anal. Chem.* **2003**, *75*, 6761–6768.
22. Huang, L. R.; Cox, E. C.; Austin, R. H.; Sturm, J. C. Continuous Particle Separation through Deterministic Lateral Displacement. *Science* **2004**, *304*, 987–990.
23. Frechette, J.; Drazer, G. Directional Locking and Deterministic Separation in Periodic Arrays. *J. Fluid. Mech.* **2009**, *627*, 379.
24. Bijeljic, B.; Mostaghimi, P.; Blunt, M. Signature of Non-Fickian Solute Transport in Complex Heterogeneous Porous Media. *Phys. Rev. Lett.* **2011**, *107*, 204502.
25. Koumoutsakos, P. Multiscale Flow Simulations using Particles. *Annu. Rev. Fluid Mech.* **2005**, *37*, 457–487.
26. Datta, S. S.; Chiang, H.; Ramakrishnan, T. S.; Weitz, D. A. Spatial Fluctuations of Fluid Velocities in Flow through a Three-Dimensional Porous Medium. *Phys. Rev. Lett.* **2013**, *111*, 064501.
27. Araújo, A. D.; Bastos, W. B.; Andrade, J. S., Jr.; Herrmann, H. J. Distribution of Local Fluxes in Diluted Porous Media. *Phys. Rev. E* **2006**, *74*, 010401.
28. He, K.; Babaye Khorasani, F.; Retterer, S. T.; Thomas, D. K.; Conrad, J. C.; Krishnamoorti, R. Diffusive Dynamics of Nanoparticles in Arrays of Nanoposts. *ACS Nano* **2013**, *7*, 5122–5130.
29. van Milligen, B.; Bons, P. Analytical Model for Tracer Dispersion in Porous Media. *Phys. Rev. E* **2012**, *85*, 011306.
30. Edwards, D.; Shapiro, M.; Brenner, H.; Shapira, M. Dispersion of Inert Solutes in Spatially Periodic, Two-Dimensional Model Porous Media. *Transp. Porous Media* **1991**, *6*, 337–358.
31. Scheven, U. M. Pore-Scale Mixing and Transverse Dispersivity of Randomly Packed Monodisperse Spheres. *Phys. Rev. Lett.* **2013**, *110*, 214504.
32. Daneyko, A.; Hlushkou, D.; Khirevich, S.; Tallarek, U. From Random Sphere Packings to Regular Pillar Arrays: Analysis of Transverse Dispersion. *J. Chromatogr. A* **2012**, *1257*, 98–115.
33. Porter, M. L.; Valdes-Parada, F. J.; Wood, B. D. Comparison of Theory and Experiments for Dispersion in Homogeneous Porous Media. *Adv. Water Resour.* **2010**, *33*, 1043–1052.
34. Michalis, V. K.; Kalarakis, A. N.; Skouras, E. D.; Burganos, V. N. Mixing within Fracture Intersections during Colloidal Suspension Flow. *Water Resour. Res.* **2009**, 45.
35. Delgado, J. Longitudinal and Transverse Dispersion in Porous Media. *Chem. Eng. Res. Des.* **2007**, *85*, 1245–1252.
36. Wang, B.; Kuo, J.; Bae, S. C.; Granick, S. When Brownian Diffusion Is not Gaussian. *Nat. Mater.* **2012**, *11*, 481–485.
37. Nagamanasa, K. H.; Gokhale, S.; Ganapathy, R.; Sood, A. K. Confined Glassy Dynamics at Grain Boundaries in Colloidal Crystals. *Proc. Natl. Acad. Sci. U.S.A.* **2011**, *108*, 11323–11326.
38. Wang, B.; Anthony, S. M.; Bae, S. C.; Granick, S. Anomalous yet Brownian. *Proc. Natl. Acad. Sci. U.S.A.* **2009**, *106*, 15160–15164.
39. deMello, A. J. Control and Detection of Chemical Reactions in Microfluidic Systems. *Nature* **2006**, *442*, 394–402.
40. He, K.; Spannuth, M.; Conrad, J. C.; Krishnamoorti, R. Diffusive Dynamics of Nanoparticles in Aqueous Dispersions. *Soft Matter* **2012**, *8*, 11933–11938.
41. Choi, C. K.; Fowlkes, J. D.; Retterer, S. T.; Siuti, P.; Iyer, S.; Doktycz, M. J. Surface Charge- and Space-Dependent Transport of Proteins in Crowded Environments of Nanotailored Posts. *ACS Nano* **2010**, *4*, 3345–3355.
42. Crocker, J. C.; Grier, D. G. Methods of Digital Video Microscopy for Colloidal Studies. *J. Colloid Interface Sci.* **1996**, *179*, 298–310.